Enhanced Reaction Engineering Approach (REA) for Modeling Continuous and Intermittent Conductive Hydro-Drying of Chili Paste (*Capsicum annuum*)

Gisselle Juri-Morales , Claudia Isabel Ochoa-Martínez , José Luis Plaza-Dorado *

Posted Date: 9 January 2026

doi: 10.20944/preprints202601.0666.v1

Keywords: intermittent drying; chili paste; heat and mass transfer; mathematical modeling; reaction engineering approach (REA)

 doi:10.20944/preprints202601.0666.v1

Article

Enhanced Reaction Engineering Approach (REA) for Modeling Continuous and Intermittent Conductive Hydro-Drying of Chili Paste (*Capsicum annuum*)

Gisselle Juri-Morales, Claudia Isabel Ochoa-Martínez and José Luis Plaza-Dorado *

GIPAB Research Group, School of Food Engineering, Universidad del Valle, Calle 13 #100-00, Santiago de Cali, Colombia

* Correspondence: jose.plaza@correounivalle.edu.co

Abstract

The chili pepper (*Capsicum annuum*) is among the most widely consumed vegetables worldwide, valued for its sensory and nutritional properties. Still, it is highly vulnerable to deterioration due to its elevated moisture content. Effective preservation strategies, such as the addition of salt combined with drying, are therefore crucial to maintaining quality and extending shelf life. This study employed a modified Reaction Engineering Approach (REA) to model the drying kinetics and temperature behavior of chili paste under continuous and intermittent conductive hydro-drying conditions. Thirty experiments were conducted, considering various salt concentrations (0, 7.5 y 15 g salt/100 g paste) , water temperatures in the hydro-dryer, and heating intermittency through on/off cycles. The modified REA model accurately predicted both moisture and temperature profiles, with determination coefficients of 0.9463 and 0.8820, respectively. In addition to direct validation with the complete dataset, cross-validation between cayenne and jalapeño varieties demonstrated the ability of the model to generalize across different formulations and structural characteristics. These results confirm the robustness of the proposed framework and its suitability as a predictive tool for heterogeneous food matrices. Overall, the model provides a reliable platform for analyzing, designing, optimizing, and controlling hydro-drying processes in semi-solid foods, supporting the development of more efficient and sustainable preservation strategies

Keywords: intermittent drying; chili paste; heat and mass transfer; mathematical modeling; reaction engineering approach (REA)

1. Introduction

Chili pepper (*Capsicum annuum*) pastes, commonly known as ají in many Latin American regions, are widely produced for sauces, seasonings, and dehydrated condiments. These pastes have high moisture content and a dense cellular matrix rich in pigments and soluble solids, which increases their perishability and complicates thermal processing. Their structural heterogeneity and compositional variability influence heat and mass transfer during dehydration, making predictive modeling particularly challenging [1,2].

Drying semi-solid foods such as pastes and purees involves coupled heat and mass transfer mechanisms that become more complex under conduction-dominated and intermittent heating conditions [3,4]. Accurate modeling requires analytical frameworks capable of representing the dynamic evolution of moisture gradients, surface temperature, and vapor concentration [3,5,6]. In the case of ají pastes, rapid pigment degradation and solute-driven modifications of water mobility further increase the need for models that reliably describe both thermal behavior and formulation effects.

 doi:10.20944/preprints202601.0666.v1

Conductive hydro-drying, derived from the Refractance Window™ concept, provides an efficient energy-transfer pathway for semi-solid systems . In this configuration, heat is transferred primarily by conduction through a thin plastic film in contact with circulating hot water, resulting in fast changes in surface temperature and moisture [7]. Unlike thin-film Refractance Window™ drying, which typically operates with layers below 1 mm, conductive hydro-drying handles product layers in the range of 1.0–1.5 mm, where radiative effects diminish and conduction becomes the dominant mechanism [8,9]. These conditions limit the predictive capacity of traditional convective drying models, which rely on assumptions of uniformity and steady-state heat transfer.

Intermittent drying introduces alternating heating and tempering phases that favor internal moisture migration, reduce thermal degradation, and improve energy management [10,11]. Heat supply can be adjusted by modifying the heating rate and temperature, as well as humidity, pressure, and the mode of energy input (convection, conduction, radiation, or microwaves). However, the rapid transitions between heating and tempering generate abrupt changes in temperature and vapor concentration, exposing inherent limitations in empirical and semi-empirical models that assume steady external conditions and minimal internal resistance. Previous research has demonstrated the benefits of applying cyclic temperature variations in intermittent drying to improve energy efficiency and product quality [12]. However, these improvements were typically implemented through predefined periodic functions [13,14], which do not capture the real thermal behavior of the circulating water or the transient interaction between the heating medium and the food matrix in conduction-based systems.

The Reaction Engineering Approach (REA) offers a mechanistically inspired but simplified framework to describe drying kinetics by linking moisture removal to an apparent activation energy term [14]. However, most reported applications rely on constant drying conditions and forced convection, without considering conductive heat transfer, solute effects, or transient heating regimes. Under intermittent operation, these assumptions restrict the ability of REA to represent rapid temperature fluctuations and shifts in evaporation resistance. Although recent studies on pastes, and other high-solids matrices emphasize the need for models that integrate structure-dependent and conduction-driven thermal behavior, REA formulations adapted to conduction-based hydro-drying under intermittent heating remain limited.

This study addresses these limitations by developing a modified REA model that incorporates conductive hydro-drying mechanisms, on/off heating cycles, and formulation effects associated with salt concentration. The objective of this study was to model the drying kinetics and temperature evolution of chili paste using the Reaction Engineering Approach (REA) under continuous and intermittent conductive hydro-drying conditions. The work was organized into three main stages: i) experimental evaluation of drying behavior under different process conditions, including salt concentration, water temperature, and heating cycles; ii) modification of REA equations to incorporate conductive hydro-drying mechanisms and intermittent energy supply; and iii) validation of the modified model using both direct comparison with experimental data and cross-validation between cayenne and jalapeño varieties.

2. Materials and Methods

2.1. Raw Material

Cayenne and red jalapeño chili pastes (Capsicum annuum) were provided by Hugo Restrepo and Cía. S.A. (Valle del Cauca, Colombia). Samples were prepared with different concentrations of sodium chloride (NaCl) (0, 7.5, and 15 g salt/100 g paste) and stored in a cold room (Dártico, Colombia) at 4 ± 2 °C.

2.2. Drying

Continuous and intermittent conductive hydro-drying experiments were conducted using an HS-50 mini dryer (Figure 1) (CEI ROBOTS®, Colombia). The effects of salt concentration, water

 doi:10.20944/preprints202601.0666.v1

temperature in the dryer, and heating intermission cycles (on/off) were evaluated. Extreme and intermediate conditions were tested for a total of 30 experiments (15 for cayenne and 15 for jalapeño, Table 1). Drying kinetics and temperature profiles were recorded for each case.

Table 1. Experiments.

Experiment	Variety	Salt concentration (g salt/100 g paste)	Intermittency (min)	Water temperature (°C)	Water temperature (K)
1	Cayenne	0	0	80	353
2	Cayenne	0	30	80	353
3	Cayenne	0	15	70	343
4	Cayenne	0	15	90	363
5	Cayenne	15	0	80	353
6	Cayenne	15	30	80	353
7	Cayenne	15	15	70	343
8	Cayenne	15	15	90	363
9	Cayenne	7.5	0	70	343
10	Cayenne	7.5	30	70	343
11	Cayenne	7.5	0	90	363
12	Cayenne	7.5	30	90	363
13	Cayenne	7.5	15	80	353
14	Cayenne	7.5	15	80	353
15	Cayenne	7.5	15	80	353
16	Jalapeño	0	0	80	353
17	Jalapeño	0	30	80	353
18	Jalapeño	0	15	70	343
19	Jalapeño	0	15	90	363
20	Jalapeño	15	0	80	353
21	Jalapeño	15	30	80	353
22	Jalapeño	15	15	70	343
23	Jalapeño	15	15	90	363
24	Jalapeño	7.5	0	70	343
25	Jalapeño	7.5	30	70	343
26	Jalapeño	7.5	0	90	363
27	Jalapeño	7.5	30	90	363
28	Jalapeño	7.5	15	80	353
29	Jalapeño	7.5	15	80	353
30	Jalapeño	7.5	15	80	353

The dryer was equipped with removable stainless-steel trays with a plastic base of 250 μm thickness (Mylar™), an insulated tank with electric resistances for water heating, a thermostat, a recirculation pump, an intermission controller, and a digital wattmeter.

 doi:10.20944/preprints202601.0666.v1

Figure 1. HS-50 mini conductive hydro-dryer.

A 1-mm-thick layer of paste was spread uniformly on the plastic film using rectangular molds (4.7 × 23.3 cm). The product mass to be dehydrated (m, g) was determined from Eq. (1) using the density of the chili pastes ρ (g/cm3), the mold area A (cm2), and the layer thickness E (cm).

$$m = (\rho)(A)(E) \quad (1)$$

2.3 Drying Kinetics

Moisture variation as a function of time was determined by weighing one tray every 5 min on an Adventurer™ ARA520 balance (OHAUS, New Jersey) until constant weight was reached, corresponding to equilibrium moisture content (EMC). The initial moisture content was determined using the oven method (AOAC 934.01). Moisture at each time (X) was calculated using Eq. (2). Experimental drying curves are provided in the supplementary material (Figure S1 and S2).

$$X = \frac{(w_t - w_b) - [(w_i - w_b)(1 - x_{im})]}{(w_i - w_b)(1 - x_{im})} \quad (2)$$

where w_t is the weight of the tray with the sample at time t (g), w_b is the weight of the empty tray (g), w_i is the initial sample weight (g), and x_{im} is the initial product moisture (g water/g wet sample).

2.4. Temperature Profiles

Temperature during drying was monitored in the second tray of the dryer using a Flir E4 thermographic camera. Measurements were taken at the center of the sample every 2 min during the first 10 min and every 4 min thereafter until the end of the drying process. Temperature profiles are available in the supplementary material (Figure S1 and S2).

2.5. Mathematical Modeling

2.5.1. Reaction Engineering Approach (REA) Model

The Reaction Engineering Approach (REA) describes drying as a mass transfer process driven by the difference in vapor concentration between the surface of the material and the bulk air. The general formulation is given by:

$$m_s \frac{dX}{dt} = -h_m A(\rho_{v,s} - \rho_{v,b}) \quad (3)$$

Here, m_s (kg) is the dry solid mass of the sample, X (kg water/kg dry solid) the average moisture content on a dry basis, t (s) the drying time, h_m (m/s) the convective mass transfer coefficient, A (m2) the exposed surface area, $\rho_{v,s}$ (kg/m^3) the vapor concentration at the sample surface, and $\rho_{v,b}$ (kg/m^3) the vapor concentration in the bulk drying air.

 doi:10.20944/preprints202601.0666.v1

A key feature of REA is that $\rho_{v,s}$ is not directly assumed as saturation at the surface temperature, but rather is corrected by an exponential term that accounts for activation energy, as introduced by [15]:

$$\rho_{v,s} = \exp\left(\frac{-\Delta E_v}{RT}\right)\rho_{v,sat_{(T)}} \tag{4}$$

where ΔE_v (kJ/mol) is the activation energy, R (J/mol K) the universal gas constant, and T (K) the sample temperature. The saturated vapor concentration $\rho_{v,sat_{(T)}}$ can be expressed as a polynomial function of temperature according to [14] (Eq. 5).

$$\begin{aligned}\rho_{v,sat(T)} = {} & 4.844 \times 10^{-9}(T-273)^4 - 1.4807 \times 10^{-7}(T-273)^3 \\ & + 2.6572 \times 10^{-5}(T-273)^2 - 4.8613 \times 10^{-5}(T-273) \\ & + 8.342 \times 10^{-3}\end{aligned} \tag{5}$$

The bulk vapor concentration $\rho_{v,b}$ is calculated from the vapor pressure, molar mass of water vapor, and drying air temperature:

$$\rho_{v,b} = \frac{P_{vapor}\, M_{vapor}}{RT_{aire}} \tag{6}$$

The vapor pressure is defined as the product of relative humidity and saturation pressure (Eq. 7), while the saturation pressure is obtained through the (1989) correlation obtained by [16] (Eq. 8).

$$P_{vapor} = (HR)(P_{sat}) \tag{7}$$

$$P_{sat} = R\exp\left[\frac{A + BT + CT^2 + DT^3 + ET^4}{FT - GT^2}\right] \tag{8}$$

where P_{vapor} (Pa) is vapor pressure, HR relative humidity, P_{sat} (Pa) saturation pressure, M_{vapor} (kg/mol) molar mass of water vapor, R (kJ/mol K) universal gas constant, and T_{aire} (K) is the bulk air temperature above the sample. Constants in Eq. (8) are defined as $R = 22105649.3$, $A = -27405.526$, $B = 97.5413$, $C = -0.146244$, $D = 1.26 \times 10^{-4}$, $E = -4.58 \times 10^{-8}$, $F = 4.34903$, and $G = 3.94 \times 10^{-3}$.

By substituting these relationships, Eq.(3) is rewritten as:

$$m_s\frac{dX}{dt} = -h_m A\left[\exp\left(\frac{-\Delta E_v}{RT}\right)\rho_{v,sat_{(T)}} - \rho_{v,b}\right] \tag{9}$$

This expression allows calculation of the activation energy (ΔE_v) as:

$$\Delta E_v = -RT\ln\left[\frac{-m_s\left(\frac{dX}{dt}\right)\frac{1}{h_m A} + \rho_{v,b}}{\rho_{v,sat_{(T)}}}\right] \tag{10}$$

The drying rate $\frac{dX}{dt}$ is determined experimentally, which enables linking ΔE_v to the average moisture content. This dependency is expressed through a functional relationship:

$$\frac{\Delta E_v}{\Delta E_{v,b}} = f(X - X_b) \tag{11}$$

where X_b is the equilibrium moisture content and $\Delta E_{v,b}$ is the equilibrium activation energy, representing the maximum value determined by equilibrium relative humidity and drying temperature. The latter is obtained from:

$$\Delta E_{v,b} = -RT_b\ln(HR_b) \tag{12}$$

with HR_b as the relative humidity of the air in equilibrium with the sample surface and T_b the corresponding temperature.

REA also accounts for the temperature profile of the sample by coupling heat transfer with moisture evaporation. The energy balance is described by:

 doi:10.20944/preprints202601.0666.v1

$$mC_p\frac{dT}{dt} = h_cA(T_b - T) + m_s\frac{dX}{dt}\Delta H_v \quad (13)$$

where m is the sample mass, C_p the specific heat, h_c the convective heat transfer coefficient and ΔH_v the latent heat of vaporization.

In practice, Eqs. (9) and (13) are solved simultaneously using numerical methods for ordinary differential equations. Together, they provide coupled predictions of both moisture loss and temperature evolution during drying, forming the basis of the original REA framework.

2.5.2. REA-Based Modeling of Conductive Hydro-Drying

Mathematical modeling was performed using the Reaction Engineering Approach (REA) with modifications to account for heat and mass transfer phenomena in continuous and intermittent conductive hydro-drying. The relationship between activation energy and average moisture content (Eq. 11) was reformulated as Eq. (14):

$$\frac{\Delta E_v}{\Delta E_{v,b}} = \alpha_1\left(\frac{X - X_b}{X_b}\right) + \alpha_2\left(\frac{\rho_{v,s}}{\rho_{v,b}}\right) + \alpha_3(C_s) \quad (14)$$

Where the first term represents the difference between product moisture (X) and equilibrium moisture (X_b), the second term accounts for the vapor concentration ratio between the food surface ($\rho_{v,s}$) and surrounding air ($\rho_{v,s}$), and the last term corresponds to salt concentration in chili paste (C_s).

By rearranging Eq. (14) and substituting into Eq. (9), the drying rate ($\frac{dX}{dt}$) was expressed as Eq. (15):

$$\frac{dX}{dt} = \frac{-h_mA}{m_s}\left[\exp\left[\frac{\left(-\alpha_1\left(\frac{X - X_b}{X_b}\right) + \alpha_2\left(\frac{\rho_{v,s}}{\rho_{v,b}}\right) + \alpha_3(C_s)\right)\Delta E_{v,b}}{RT}\right]\rho_{v,sat(T)} - \rho_{v,b}\right] \quad (15)$$

Prediction of temperature behavior ($\frac{dT}{dt}$) was achieved by modifying Eq. (13) to incorporate a conductive heat transfer term $\left(kA\frac{(T_w - T)}{d}\right)$ through the plastic film (Eq. 16):

$$\frac{dT}{dt} = \frac{1}{mC_p}\left[h_cA(T_b - T) + kA\frac{(T_w - T)}{d} + m_s\frac{dX}{dt}\Delta H_v\right] \quad (16)$$

where k (W/m·K) represents the thermal conductivity of the Mylar plastic film, T_w (K) the water temperature in the hydro-dryer, T (K) the sample temperature, and d (m) the sample thickness.

Water temperature in the hydro-dryer T_w was constant in continuous mode. For the intermittent mode, two differential equations were defined: one for the heating phase (Eq. 17) and another for the cooling phase (Eq. 18), taking into account convection between the water and the food.

$$\frac{dT_w}{dt} = \frac{1}{m_wC_{p,w}}\left[h_{w,on}A(T_e - T_w)\right] \quad (17)$$

$$\frac{dT_w}{dt} = -\frac{1}{m_wC_{p,w}}\left[h_{w,off}A(T_w - T)\right] \quad (18)$$

where m_w (kg) accounts for the mass of water used during drying, $C_{p,w}$ (J/kg·K) is the specific heat of water, $h_{w,on}$ (m/s) is the convective mass transfer coefficient under heating, $h_{w,off}$ (m/s) the convective mass transfer coefficient under cooling, and T_e (K) the drying temperature.

The coefficients α_1, α_2, and α_3, together with the variables h_m, h_c, $h_{w,on}$, $h_{w,off}$ and k were treated as adjustable parameters of the model. Table 2 presents the values of the fixed variables used

 doi:10.20944/preprints202601.0666.v1

in both equations, while Table 3 summarizes the dependent variables of chili paste for each experiment, categorized by salt concentration and variety. Additional variables, such as equilibrium moisture content (X_b), sample mass (m), equilibrium air temperature above the sample (T_b), and equilibrium relative humidity near the sample surface (HR_b), are provided in the supplementary material (Table S1 and Table S2).

Table 2. Fixed Parameters used in the mathematical model.

Name	Variable	Unit	Value
Sample surface area	A	m^2	0.011
Universal gas constant	R	J/mol K	8.314
Molar mass of vapor	M_{vapor}	kg/mol	0.018
Sample thickness	d	m	0.001
Latent heat of vaporization of water at sample temperature	ΔH_v	J/kg	2.35×10^6 - 2.48×10^6
Water mass	m_w	kg	6.000
Specific heat of water	$C_{p,w}$	J/kg K	4180

Table 3. Dependent Parameters of Chili Paste.

Chili Paste variety	Salt concentration (g of salt/100 g of paste)	Name	Variable	Unit	Value
Cayenne	0	Dry solid mass of the sample	m_s	kg	0.002
	7.5				0.003
	15				0.003
Jalapeño	0				0.001
	7.5				0.002
	15				0.003
Cayenne	0	Specific heat of the sample	C_p	J/kg	3885
	7.5				3664
	15				3499
Jalapeño	0				3941
	7.5				3703
	15				3567

2.6. Parameter Estimation and Model Validation

The differential equations for moisture and temperature (Eqs. 15-18) were solved simultaneously in MATLAB R2025a using the ode15s solver. A multistart strategy was implemented by initializing 100 different starting points for the solution space, ensuring that the optimization did not converge to local minima. Parameter estimation (θ, adjustable parameters) was performed through the Nelder–Mead simplex optimization algorithm (fminsearch function) to minimize the objective or "cost" function based on the least squares criterion, which corresponds to the sum of squared differences between model predictions and experimental measurements (Eq. 19).

$$J(\theta) = \sum_{j=1}^{n} \sum_{i=1}^{N} (y_{ij}(\theta) - y_{mes,ij})(y_{ij}(\theta) - y_{mes,ij})^T \quad (19)$$

 doi:10.20944/preprints202601.0666.v1

Where $J(\theta)$ is objective or cost function of the model, θ vector of parameters to be identified, $y_{ij}(\theta)$ vector of simulated variables at instant i of experiment j and $y_{mes,ij}$ vector of experimental measurements at instant i of experiment j.

To analyze the sensitivity of the model outputs with respect to the estimated parameters, (X), (T) and (T_w) were defined as the system outputs y_i with $i = 1{:}3$, while the adjustable parameters were denoted by θ_j with $j = 1{:}8$. The time evolution of the 3×8 sensitivity functions $\partial y_i / \partial \theta_j$ was computed by differentiating the modified REA equations with respect to each parameter:

$$\frac{d}{dt}\left(\frac{\partial y_i}{\partial \theta_j}\right) = \frac{\partial f_i}{\partial \theta_j} + \sum_{k=1}^{m} \frac{\partial f_i}{\partial y_k}\frac{\partial y_k}{\partial \theta_j} \; for\; i = 1{:}3,\; j = 1{:}8,\; m = \dim(y) = 3 \tag{20}$$

Here, $f_i(y, \theta, t)$represent the right-hand terms of the coupled REA-based drying equations for moisture (Eq. 15) and temperature (Eqs. 16–18). The sensitivity functions were numerically integrated simultaneously with the state variables using the same solver and time employed for parameter estimation.

These sensitivity functions were then used to compute the lower bound of the parameter-estimation variance (Cramer–Rao bound) through the Fisher information matrix:

$$F = \sum_{j=1}^{n}\sum_{i=1}^{N}\left(\frac{\partial y_{ij}}{\partial \theta}\right)^{T} Q_{ij}^{-1}\left(\frac{\partial y_{ij}}{\partial \theta}\right) \tag{21}$$

where $y_{ij} = [X_{ij}, T_{ij}]$ corresponds to the measured moisture and temperature at time i in experiment j, and Q_{ij} denotes the covariance matrix of the experimental measurements. The diagonal entries of the inverse of the Fisher matrix provide the minimum achievable estimation variance:

$$\sigma_{\theta_i}^2 = S_{ii}, S = F^{-1} \tag{22}$$

Finally, the confidence intervals (CI) for the estimated parameters, calculated at a 95% confidence level, are as follows:

$$CI = \theta_i \pm 2\,\sigma_{\theta_i} \tag{23}$$

where $\theta^T = [\alpha_1\; \alpha_2\; \alpha_3\; h_m\; h_c\; k\; h_{w,on}\; h_{w,off}\;]$.

To examine how each pair of parameters is related, the correlation matrix can be derived using the covariance matrix S, which corresponds to the inverse of the Fisher information matrix:

$$COR(\theta_i, \theta_j) = \frac{S_{d\,ij}}{\sqrt{S_{d\,ii}}\sqrt{S_{d\,jj}}} \tag{24}$$

The correlation matrix shows that if two parameters have no relationship, their correlation coefficient will be zero. Conversely, a coefficient of 1 indicates a perfect positive relationship between them, while a value of –1 reflects a completely negative relationship. For better visualization, a heat-map representation of the absolute values of the correlation coefficients was generated.

A multi-start strategy was implemented to reduce the likelihood of convergence to local minima. One hundred pseudo-random initial parameter vectors were generated within the bounds listed in Table 4 and used as independent starting points for the Nelder–Mead optimization. A correlation matrix was also computed from the normalized sensitivity functions to examine parameter interdependence during estimation.

The ranges used to initialize the adjustable parameters in the multistart strategy are summarized in Table 4.

Table 4. Parameter initialization ranges used in the multistart strategy.

Parameter	Unit	Range

 doi:10.20944/preprints202601.0666.v1

α_1	–	–1.5 to 1.5
α_2	–	0.0 to 1.0
α_3	–	–2.0 to 0.0
h_m	m/s	10^{-4} to 10^{-2}
h_c	W/m²·K	50 to 500
$h_{w,on}$	m/s	10^{-4} to 10^{-2}
$h_{w,off}$	m/s	10^{-5} to 10^{-3}
k	W/m·K	0.001 to 0.1

In cross-validation, two independent tests were carried out. In the first step, the model was calibrated using data from 15 cayenne experiments and then applied to predict the drying behavior of 15 jalapeño experiments. In the second step, calibration was performed using jalapeño data to predict the drying behavior of cayenne experiments. This bidirectional approach provided a more rigorous evaluation of the model's predictive capacity under conditions not directly used for calibration, confirming both its robustness and generalization potential.

The goodness of fit between experimental and simulated values was evaluated through the determination coefficient (R^2), calculated for each simulated variable in both direct and cross-validation of the model:

$$R^2 = 1 - \frac{\sum_{j=1}^{n}\sum_{i=1}^{N}\left(y_{ij}(\theta) - y_{mes,ij}\right)^T\left(y_{ij}(\theta) - y_{mes,ij}\right)}{\sum_{j=1}^{n}\sum_{i=1}^{N}\left(y_{ij}(\theta) - \bar{y}_{mes}\right)^T\left(y_{ij}(\theta) - \bar{y}_{mes}\right)} \quad (25)$$

3. Results

3.1 Parameter Estimation

The adjustable parameters obtained from the parametric estimation are presented in Table 5.

The variation in moisture content and temperature behavior of chili pastes during drying is shown in Figures 2 and 3, where blue circles represent the experimental data and the red line represents the predictions of the REA model.

Table 5. Parameter values (θ = 8) identified through direct validation (all experiments) and cross-validation between cayenne and jalapeño varieties.

Parameter	Direct validation (Experiments 1 to 30)
	Adjusted value
α_1	-0.106
α_2	0.342
α_3	-0.933
h_m (m/s)	3.097×10^{-5}
h_c (W/m²K)	180.006
$h_{w,on}$ (W/m²K)	648.999
$h_{w,off}$ (W/m²K)	290.957
k (W/m K)	0.008
$R^2_{moisture}$	0.946
$R^2_{temperature}$	0.882
SSE[a]	11277.230

[a]SSE are calculated from Eq. 18 on the whole set of experiments

Figures 2 and 3 compare experimental values with predictions obtained from the modified REA model, revealing a high level of agreement for both key process variables: moisture content and temperature. The differences between the experimental data and simulations were minimal,

 doi:10.20944/preprints202601.0666.v1

indicating that the mathematical formulation successfully captured the main dynamics of the system. The global determination coefficients (R^2 = 0.9463 for moisture and R^2 = 0.8820 for temperature) provide quantitative confirmation of the ability of the model to describe system behavior under different operating. This outcome is particularly significant given the inherent complexity of drying semi-solid food matrices, where coupled phenomena of mass transfer, heat transfer, and structural transformations interact. The model reproduced the kinetics of moisture loss and the thermal evolution of the product with high accuracy, including transient processes driven by on/off heating cycles characteristic of intermittent operation.

 doi:10.20944/preprints202601.0666.v1

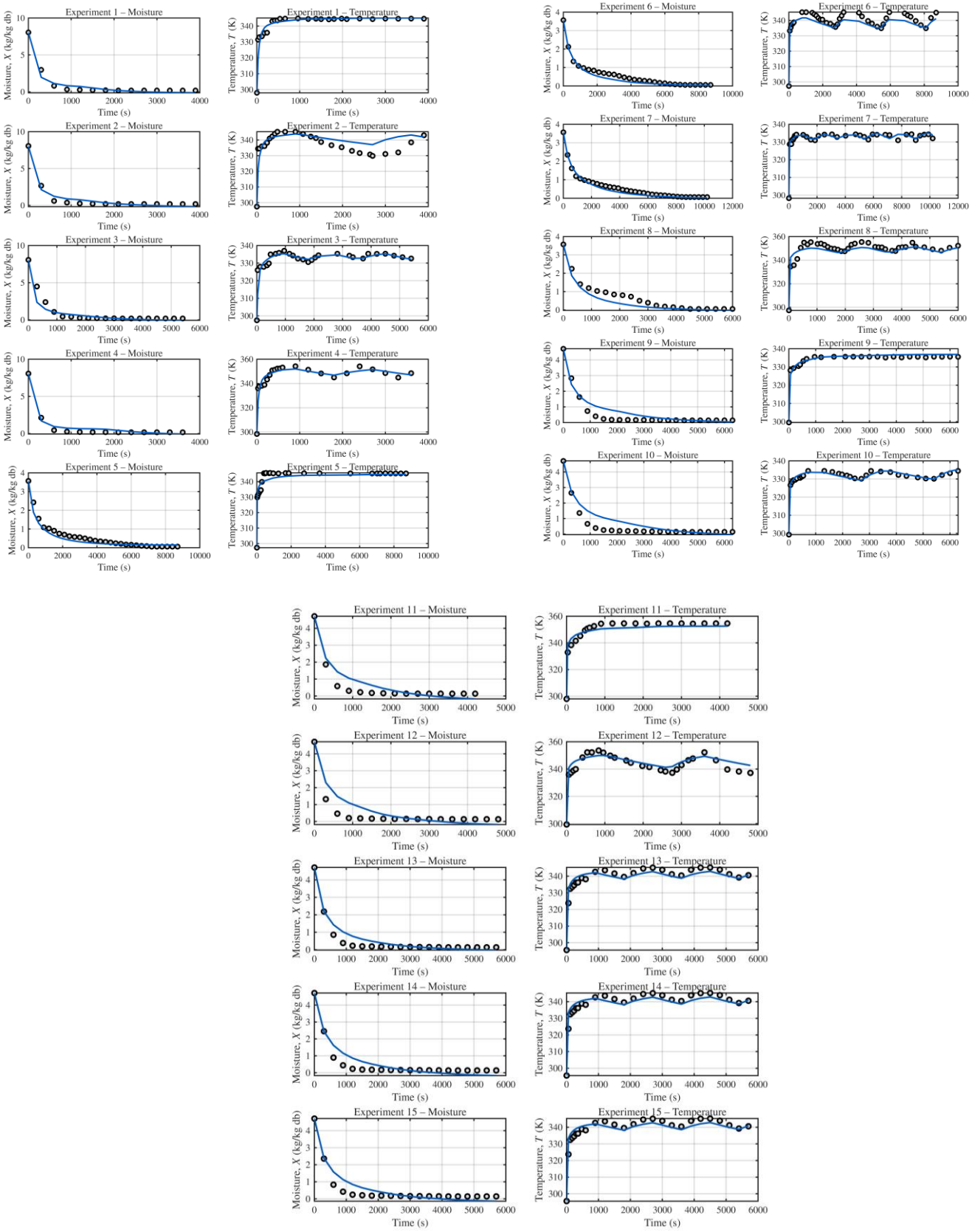

Figure 2. Modeled moisture and temperature behaviors of cayenne pepper paste as a function of drying time.

 doi:10.20944/preprints202601.0666.v1

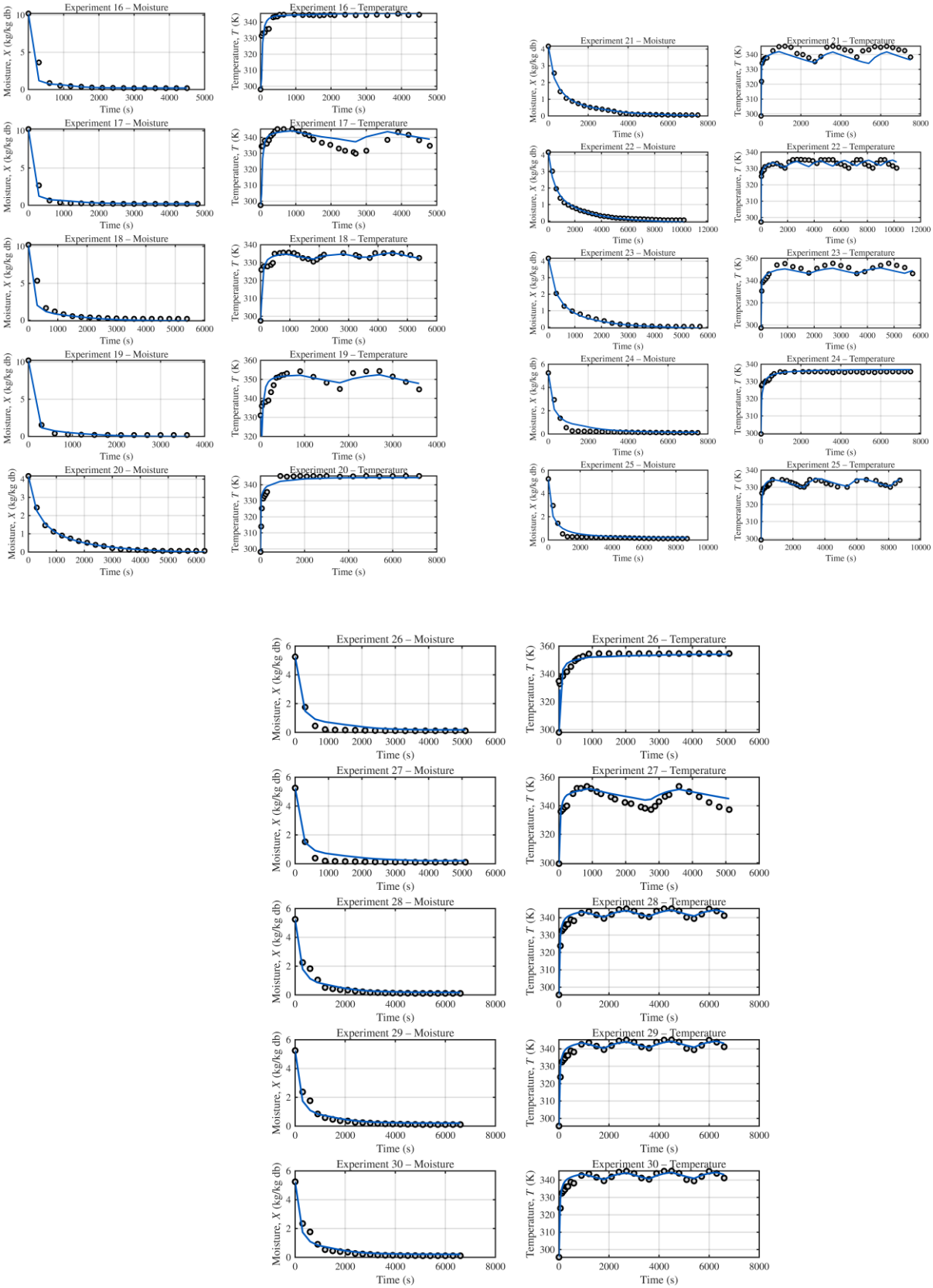

Figure 3. Modeled moisture and temperature behaviors of jalapeño chili paste as a function of drying time.

3.2. *Sensitivity Analysis*

The confidence intervals obtained for the estimated parameters are presented in Table 6. A heat-map representation of the absolute values of the correlation coefficients is shown in Fig. 4.

 doi:10.20944/preprints202601.0666.v1

Additionally, the numerical values of the correlation matrix are provided in the supplementary material (Table S3).

Table 6. Confidence intervals for the estimated parameters.

Parameter	Lower bound (lb)	Upper bound (ub)
α_1	−0.113	0
α_2	0.322	0.362
α_3	−2.18	2.16
h_m (m/s)	1.25×10^{-5}	4.94×10^{-5}
h_c (W/m^{2}K)	1.53×10^{2}	2.07×10^{2}
k (W/m K)	0.00642	0.00815
$h_{w,off}$ (W/m^{2}K)	2.55×10^{2}	3.27×10^{2}
$h_{w,on}$ (W/m^{2}K)	5.16×10^{2}	7.82×10^{2}

Figure 4 shows the heat-map representation of the absolute values of the parameter correlation matrix, illustrating the degree of linear dependence among the estimated parameters.

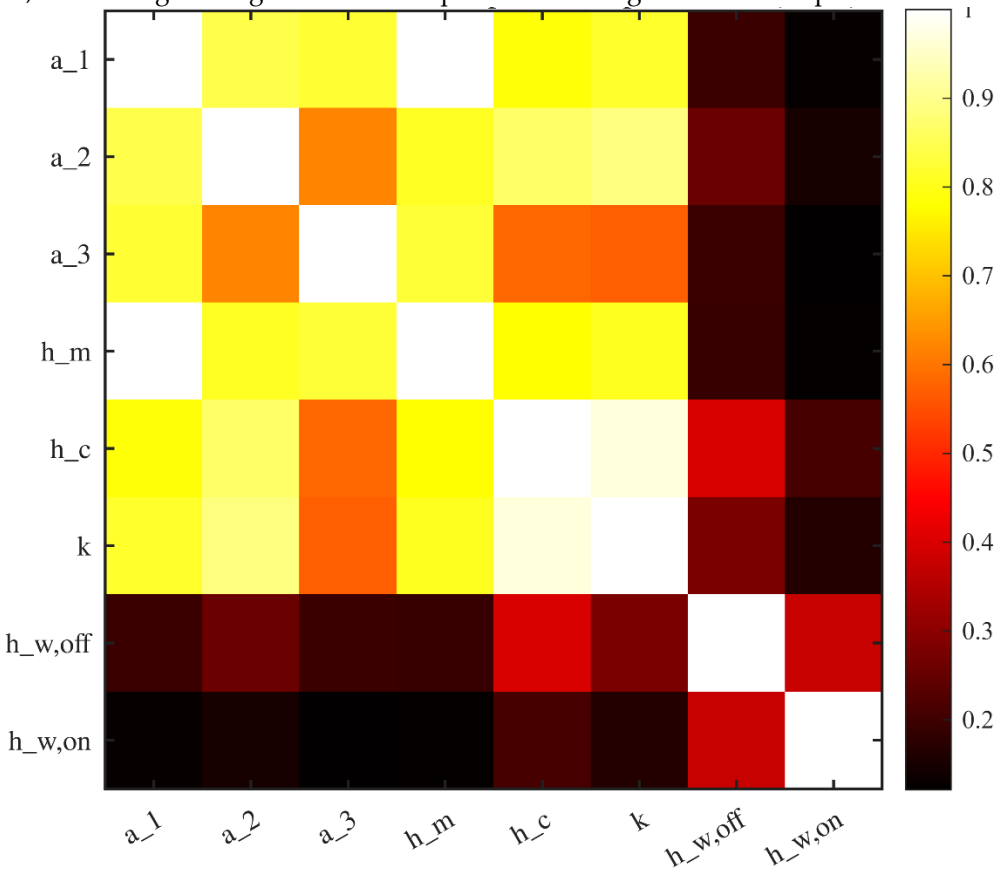

Figure 4. Absolute correlation heat-map between model parameters.

3.3. Direct and Cross-Validation

The accuracy of the model was examined through direct and cross-validation. In direct validation, parameter estimation was performed with the full dataset of 30 experiments. At the same time, cross-validation alternated between the cayenne and jalapeño datasets to predict the other variety (the modeled behaviors are provided in the supplementary material Figure S3 and S4). The results of both validation procedures are presented in Table 7.

 doi:10.20944/preprints202601.0666.v1

Table 7. Parameter values (θ = 8) identified through direct validation (all experiments) and cross-validation between cayenne and jalapeño varieties.

Parameter	Direct validation (Experiments 1 to 30)	Cross-validation (Experiments 1 to 15)	Cross-validation (Experiments 16 to 30)
	Adjusted value	Adjusted value	Adjusted value
α_1	-0.106	-0.116	-0.104
α_2	0.342	0.384	0.346
α_3	-0.933	-0.008	-1.574
h_m (m/s)	3.097×10^{-5}	3.337×10^{-5}	2.140×10^{-5}
h_c (W/m^2K)	180.006	80.149	217.591
$h_{w,on}$ (W/m^2K)	648.999	628.401	710.640
$h_{w,off}$ (W/m^2K)	290.957	486.132	272.280
k (W/m K)	0.008	0.004	0.008
$R^2_{moisture}$	0.946	0.946	0.933
$R^2_{temperature}$	0.882	0.724	0.891
SSE	11277.230	23273.700	10472.410

a. $R^2_{moisture}$ and $R^2_{temperature}$ were calculated from Eq. (20) using the complete set of experiments, cayena and jalapeño.

b. The sum of squared errors (SSE) was calculated from Eq. (19) using the complete set of experiments, cayena, and jalapeño.

4. Discussion

4.1. Behavior of the Modified REA Formulation and Comparison with Previous REA Studies

The modified REA formulation developed in this study incorporates independent differential equations to describe the heating and cooling phases of the water bath. This contrasts with previous approaches in intermittent drying, where oscillatory changes in air temperature or humidity were imposed using predefined periodic functions (e.g., sinusoidal or square-wave profiles) [12,17]. The proposed model incorporates water mass, heat capacity, and instantaneous heat exchange with the product, which removes simplified assumptions that fail to represent fluid dynamics or the thermal inertia of the system.

This capability is particularly relevant when compared with REA studies applied to intermittent convective drying under externally imposed variations. For example, Putranto [14] demonstrated that REA can effectively reproduce moisture and temperature profiles under time-varying humidity and temperature, although the drying medium was controlled externally rather than arising from coupled water–sample interactions. Similarly, Kowalski & Pawłowski [13] reported that the internal temperature of kaolin cylinders remained practically uniform during drying, meaning that no significant temperature gradients developed inside the material. This behavior indicates that heat was redistributed quickly within the sample compared with the rate at which it was exchanged with the environment. Under these conditions, the product can be treated as a thermally homogeneous body, which allows the use of simplified models that represent the material as having a single, spatially average temperature. Their work also benchmarked REA predictions against diffusion-based models, showing comparable or even superior accuracy for moisture evolution.

In contrast with these systems, chili pastes introduce substantial challenges due to structural complexity, compositional variability, and non-uniform layer thickness [18]. Even under these conditions, the modified REA model maintains a predictive capacity comparable to that reported for

 doi:10.20944/preprints202601.0666.v1

simpler matrices such as mineral systems, starch-based gels, or thin food tissues [19]-[20]. These results indicate that coupling the REA framework with dynamic boundary conditions extends its applicability to a broader range of semi-solid food materials.

4.2. Parameter Identification, Variance Analysis and Global Sensitivity Interpretation

The estimated parameters showed coherent mechanistic behavior when evaluated collectively. The activation-energy parameters α_1, α_2, and α_3 capture the combined influences of moisture availability, vapor driving force, and salt concentration. The narrow confidence intervals of α_1 and α_2 indicate that the dataset strongly constrains the mechanisms associated with removal of free water and reduction of vapor gradients, consistent with classical profiles of the transition between constant- and falling-rate periods in drying [19,21]. Comparable trends have been reported in other REA applications, where moisture mobility dominates the activation-energy behavior during the falling-rate regime [14].

On the other hand, the broader uncertainty observed in α_3 aligns with evidence showing that compositional variables such as solute concentration have intertwined effects with moisture-related phenomena, making their individual estimation more difficult in lumped models [20,22]. This indicates that formulation-specific effects, while influential, require targeted experimentation to be decoupled from moisture-driven mechanisms.

The strong correlation between h_m and h_c confirms their shared influence on the surface flux, a behaviour commonly observed in conductive and convective REA implementations [23,24]. Despite this correlation, variance analysis indicated narrow uncertainty bounds for both coefficients, showing that their combined effect is well captured by the simultaneous fitting of temperature and moisture profiles. Meanwhile, the composite thermal conductivity k behaved as a stable parameter, though its lower magnitude compared with reported multilayer systems [23,25] suggests that it may compensate for moisture-dependent thermal properties not explicitly included in the model.

The water-side coefficients $h_{w,\mathrm{on}}$ and $h_{w,\mathrm{off}}$ presented broader confidence intervals, consistent with the limited independent observability of water temperature transients. Nonetheless, their influence on the global sensitivity indices was moderate, confirming that internal moisture and energy dynamics dominate system behavior, while water-side heat transfer modulates the amplitude and timing of thermal oscillations [23].

4.3. Cross-Validation and Implications for Model Robustness

Direct validation across 30 experiments showed coherent parameter estimates and high predictive performance, with moisture and temperature profiles reproduced within typical ranges reported for conductive drying systems [23,24]. The goodness-of-fit indicators confirmed this robustness: R^2 for moisture reached 0.946, while R^2 for temperature was 0.882, indicating that the model effectively captured both moisture kinetics and temperature evolution. The SSE value (11277.230) indicated a good agreement between predictions and experimental data.

Cross-validation introduced a more stringent scenario by confronting the model with varietal differences in composition, pigment distribution, solids content, and physical structure. The observed shift in parameters such as α_3 and the reduction in h_c highlight the sensitivity of thermal behavior to variety. This outcome is consistent with literature showing that thermal properties such as conductivity and heat capacity vary markedly with composition and moisture content in pastes and gels [19–22,26]. In REA studies on kaolin and polymer gels, comparable decreases in temperature predictive accuracy have been reported when the physical structure differed between calibration and validation conditions [14].

The decline in R^2 for temperature under cross-validation thus reflects inherent structural and compositional variability between chili varieties rather than deficiencies of the REA framework. This suggests that future calibrations should incorporate multi-variety datasets to ensure generalization in heterogeneous food matrices.

 doi:10.20944/preprints202601.0666.v1

4.2. Model Limitations and Opportunities for Improvement

Several structural limitations emerge during the analysis. Sensitivity to chili variety highlights the influence of compositional and structural differences on heat transfer, consistent with observations in heterogeneous matrices such as starch-based gels and mineral pastes [14,22]. Possible heterogeneity in layer thickness introduces additional variability in conduction pathways that a macroscopic representation cannot represent explicitly. The assumption of constant thermal conductivity prevents the model from representing known moisture-dependent thermophysical changes, particularly during early heating and late cooling stages [19,21] . Additionally, the behavior of bound water is represented implicitly in the activation-energy formulation but may require explicit modelling to capture the sharp increase in resistance at low moisture contents.

These limitations align with known constraints of REA in complex materials, but they also provide a clear direction for improvement. Incorporating moisture-dependent thermal properties, correcting for spatial variability, or coupling REA with simplified diffusion terms could further enhance model fidelity. Such extensions would broaden the applicability of REA to a wider range of semi-solid food systems and increase predictive accuracy under realistic processing conditions.

5. Conclusions

The modified Reaction Engineering Approach (REA) developed in this study accurately represented the coupled moisture and temperature behavior of chili pastes during conductive hydro-drying under continuous and intermittent conditions. The model achieved strong agreement with experimental data in both direct validation and cross-validation across two chili varieties, confirming its robustness under structural and compositional variability. The sensitivity analysis showed that parameters associated with moisture availability and vapor driving force were the dominant contributors to model behavior, while coefficients linked to salt effects and water-side heat transfer exhibited greater uncertainty. These findings highlight the central role of moisture-dependent energetic mechanisms in hydro-drying and indicate which parameters require improved experimental resolution. Limitations remained in the assumption of constant thermophysical properties, the lack of explicit representation of variations in sample thickness, and the indirect treatment of bound-water effects. Addressing these aspects—together with experiments designed to isolate compositional influences—would further enhance model generalization. Future extensions may integrate moisture-dependent thermal properties or simplified spatial corrections to broaden the applicability of REA-based models in complex semi-solid foods.

Supplementary Materials: The following supporting information can be downloaded at the website of this paper posted on Preprints.org.

Author Contributions: Conceptualization, G.J.-M., C.I.O.-M. and J.L.P.-D.; methodology, G.J.-M. and J.L.P.-D.; software, G.J.-M. and J.L.P.-D.; validation, G.J.-M. and J.L.P.-D.; formal analysis, G.J.-M. and J.L.P.-D.; investigation, G.J.-M.; resources, C.I.O.-M. and J.L.P.-D.; data curation, G.J.-M.; writing—original draft preparation, G.J.-M.; writing—review and editing, G.J.-M., C.I.O.-M. and J.L.P.-D.; visualization, G.J.-M.; supervision, C.I.O.-M. and J.L.P.-D.; project administration, C.I.O.-M. and J.L.P.-D.; funding acquisition, C.I.O.-M. and J.L.P.-D. All authors have read and agreed to the published version of the manuscript.

Funding: Support for doctoral student, project: Effect of intermittent hydro-conductive drying on the quality of dehydrated chili peppers and energy consumption of the process, CI21188, Universidad del Valle.

Data Availability Statement: All data supporting the findings of this study are available within the paper and its Supplementary Information.

Acknowledgments: The authors would like to thank Hugo Restrepo and Cia S.A. for supplying the chili paste and the Universidad del Valle for funding this research through an internal call for proposals.

Conflicts of Interest: The authors declare no conflicts of interest.

 doi:10.20944/preprints202601.0666.v1

References

1. Tan, J.; Li, M.F.; Li, R.; Jiang, Z.T.; Tang, S.H.; Wang, Y. Front-Face Synchronous Fluorescence Spectroscopy for Rapid and Non-Destructive Determination of Free Capsanthin, the Predominant Carotenoid in Chili (Capsicum Annuum L.) Powders Based on Aggregation-Induced Emission. *Spectrochim. Acta - Part A Mol. Biomol. Spectrosc.* **2021**, *255*, 1–9, doi:10.1016/j.saa.2021.119696.
2. Getahun, E.; Gabbiye, N.; Delele, M.A.; Fanta, S.W.; Gebrehiwot, M.G.; Vanierschot, M. Effect of Maturity on the Moisture Sorption Isotherm of Chili Pepper (Mareko Fana Variety). *Heliyon* **2020**, *6*, 1–14, doi:10.1016/j.heliyon.2020.e04608.
3. Verma, D.K.; Thakur, M.; Srivastav, P.P.; Karizaki, V.M.; Suleria, H.A.R. Effects of Drying Technology on Physiochemical and Nutritional Quality of Fruits and Vegetables. In *Emerging Thermal and Nonthermal Technologies in Food Processing*; Apple Academic Press, 2020; pp. 69–116.
4. Rajoriya, D.; Shewale, S.R.; Hebbar, H.U. Refractance Window Drying of Apple Slices: Mass Transfer Phenomena and Quality Parameters. *Food Bioprocess Technol.* **2019**, *12*, 1646–1658, doi:10.1007/s11947-019-02334-7.
5. Khan, M.I.H.; Welsh, Z.; Gu, Y.; Karim, M.A.; Bhandari, B. Modelling of Simultaneous Heat and Mass Transfer Considering the Spatial Distribution of Air Velocity during Intermittent Microwave Convective Drying. *Int. J. Heat Mass Transf.* **2020**, *153*, doi:10.1016/j.ijheatmasstransfer.2020.119668.
6. Arpaci, E.; Atayılmaz, Ş.Ö.; Gemici, Z. Exploring Mathematical Modeling and CFD in Convective Drying of Fruits and Vegetables: A Review. *Food Bioprocess Technol.* **2025**, *18*, 3195–3222, doi:10.1007/s11947-024-03627-2.
7. Waghmare, R. Refractance Window Drying: A Cohort Review on Quality Characteristics. *Trends Food Sci. Technol.* 2021, *110*, 652–662.
8. Ortiz-Jerez, M.J.; Ochoa-Martínez, C.I. Heat Transfer Mechanisms in Conductive Hydro-Drying of Pumpkin (Cucurbita Maxima) Pieces. *Dry. Technol.* **2015**, *33*, 965–972, doi:10.1080/07373937.2015.1009538.
9. Ortiz, M.J.; Ochoa Martínez, C.I. Efecto de Las Condiciones Del Hidrosecado Sobre El Encogimiento de Trozos de Zapallo (Cucurbita Maxima). *Ing. y Compet.* **2018**, *20*, 37–44, doi:10.25100/iyc.v20i2.5809.
10. Zhu, H. kun; Yang, L.; Fang, X. fa; Wang, Y.; Li, D.; Wang, L. jun Effects of Intermittent Radio Frequency Drying on Structure and Gelatinization Properties of Native Potato Flour. *Food Res. Int.* **2021**, *139*, doi:10.1016/j.foodres.2020.109807.
11. Zotti-Sperotto, N.C.; de Ávila, M.B.R.; de Souza, R.A.; Melo, E. de C.; Governici, J.L.; Gonzaga, D.A.; Fonseca, M.C.M.; Carneiro, A.P. d. S.; Demuner, A.J.; Pinheiro, P.F.; et al. Intermittent Drying of Lippia Origanoides H.B.K. Leaves and Schinus Terebinthifolius Raddi Fruits. *Ind. Crops Prod.* **2021**, *161*, 1–14, doi:10.1016/j.indcrop.2020.113152.
12. Kumar, C.; Karim, M.A.; Joardder, M.U.H. Intermittent Drying of Food Products: A Critical Review. *J. Food Eng.* 2014, *121*, 48–57.
13. Kowalski, S.J.; Pawłowski, A. Modeling of Kinetics in Stationary and Intermittent Drying. *Dry. Technol.* **2010**, *28*, 1023–1031, doi:10.1080/07373937.2010.497095.
14. Putranto, A.; Chen, X.D.; Devahastin, S.; Xiao, Z.; Webley, P.A. Application of the Reaction Engineering Approach (REA) for Modeling Intermittent Drying under Time-Varying Humidity and Temperature. *Chem. Eng. Sci.* **2011**, *66*, 2149–2156, doi:10.1016/j.ces.2011.02.025.
15. Chen, X.D.; Chen, N.X. Preliminary Introduction to a Unified Approach to Modeling Drying and Equilibrium Isotherms of Moist Porous Solids. *Proc. Chemeca, Rotorua, New Zeal.* **1997**.
16. Ambrose, D.; Walton, J. Vapour Pressures up to Their Critical Temperatures of Normal Alkanes and 1-Alkanols. **1989**, *61*, 1395–1403, doi:doi:10.1351/pac198961081395.
17. Chua, K.J.; Chou, S.K.; Ho, J.C.; Mujumdar, A.S.; Hawlader, M.N.A. Cyclic Air Temperature Drying of Guava Pieces: Effects on Moisture and Ascorbic Acid Contents. *Food Bioprod. Process. Trans. Inst. Chem. Eng. Part C* **2000**, *78*, 72–78, doi:10.1205/096030800532761.
18. Zhang, R.; Chen, G.; Yang, B.; Wu, Y.; Du, M.; Kan, J. Insights into the Stability of Carotenoids and Capsaicinoids in Water-Based or Oil-Based Chili Systems at Different Processing Treatments. *Food Chem.* **2021**, *342*, 1–10, doi:10.1016/j.foodchem.2020.128308.

 doi:10.20944/preprints202601.0666.v1

19. Abdullah, Z.; Taip, F.S.; Kamal, S.M.M.; Abdul Rahman, R.Z. Nonlinear Model-Based Inferential Control of Moisture Content of Spray Dried Coconut Milk. *Foods* **2020**, *9*, 1–22, doi:10.3390/foods9091177.
20. Moreira, R.; Chenlo, F.; Chaguri, L.; Vázquez, G. Air Drying and Colour Characteristics of Chestnuts Pre-Submitted to Osmotic Dehydration with Sodium Chloride. *Food Bioprod. Process.* **2011**, *89*, 109–115, doi:https://doi.org/10.1016/j.fbp.2010.03.013.
21. Parikh, D.M. Solids Drying: Basics and Applications Available online: https://www.chemengonline.com/solids-drying-basics-and-applications/?printmode=1 (accessed on 7 October 2025).
22. Haque, M.A.; Hosain, M.; Putranto, A.; Adhikari, B. Drying and Denaturation Kinetics of Beta-Lactoglobulin during Convective Drying. *J. Food Eng.* **2018**, *237*, 9–17, doi:10.1016/j.jfoodeng.2018.05.018.
23. Cengel, Y.A.; Ghajar, A.J. *Heat and Mass Transfer*; Mcgraw-Hill Education-Europe, London, 2014; ISBN 9814595276.
24. Geankoplis, C. *Transport Processes and Separation Process Principles (Includes Unit Operations)*; Prentice Hall Press, 2003; ISBN 013101367X.
25. Choi, Y.; Okos, M.R. Effects of Temperature and Composition on the Thermal Properties of Foods. *Food Eng. Process Appl., Transp. phenomena., Elsevier* **1986**, *1*, 99–101.
26. Rajoriya, D.; Bhavya, M.L.; Hebbar, H.U. Impact of Process Parameters on Drying Behaviour, Mass Transfer and Quality Profile of Refractance Window Dried Banana Puree. *LWT* **2021**, *145*, 1–55, doi:10.1016/j.lwt.2021.111330.